Vol. 27 • No. 6 • February 10 • 2017

www.afm-journal.de

ADVANCED FUNCTIONAL MATERIALS

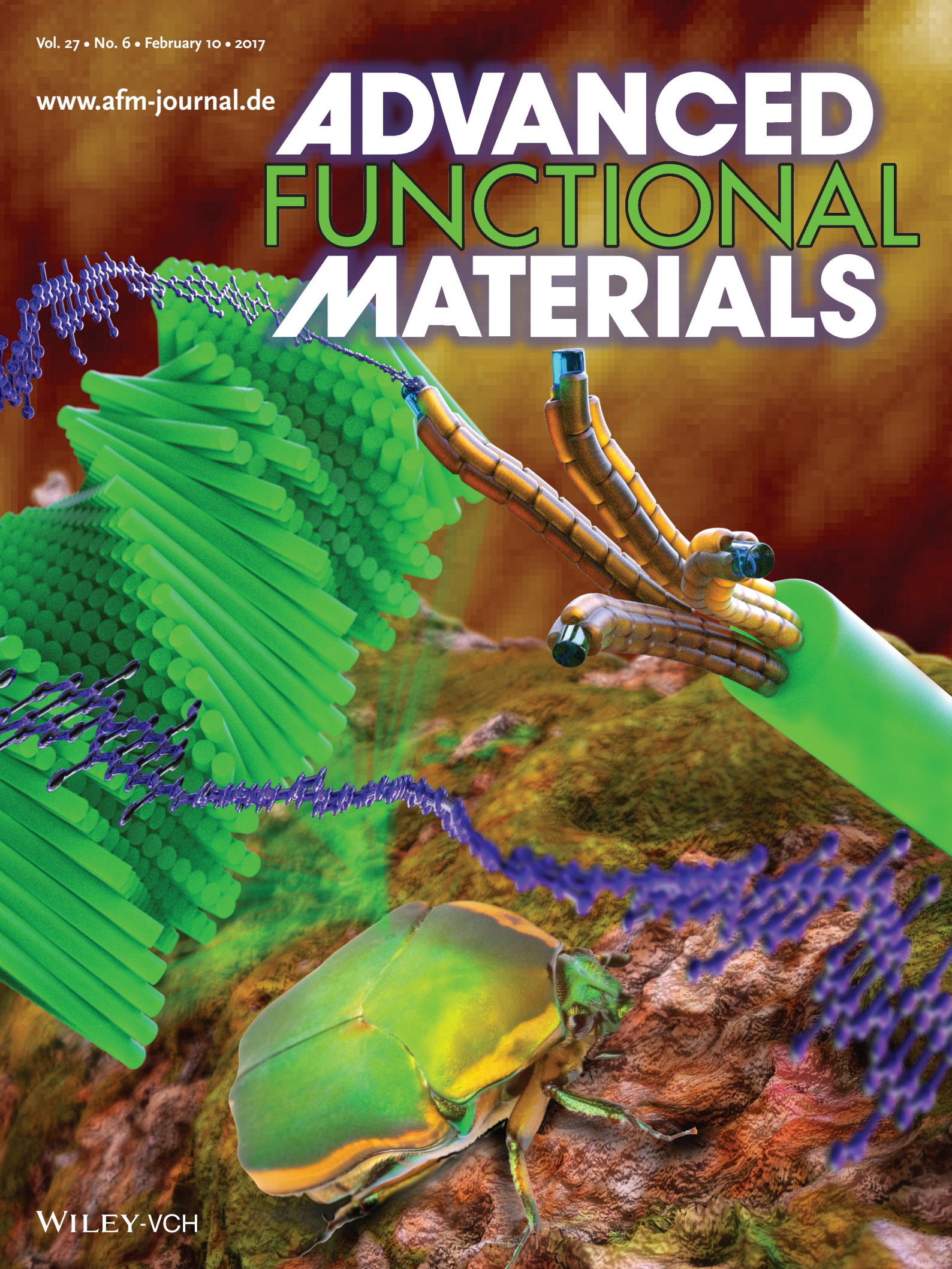

WILEY-VCH

AFM Identification of Beetle Exocuticle: Bouligand Structure and Nanofiber Anisotropic Elastic Properties

*Ruiguo Yang, Alireza Zaheri, Wei Gao, Cheryl Hayashi, and Horacio D. Espinosa**

One of the common architectures in natural materials is the helicoidal (Bouligand) structure, where fiber layers twist around a helical screw. Despite the many studies that have shown the existence of Bouligand structures, methods for nanoscale structural characterization and identification of fiber mechanical properties remain to be developed. In this study, we used the exocuticle of Cotinis mutabilis (a beetle in the Cetoniinae) as a model material to develop a new experimental-theoretical methodology that combines atomic force microscopy-based nanoindentation and anisotropic contact mechanics analysis. Using such methodology, we studied both the helicoidal structure and the mechanical properties of its constituent fibers. The twist angle between the layers was found to be in the range of 12°–18° with a pitch size of 220 nm for the helicoidal pattern. In addition, the constituent fiber diameter was measured to be approximately 20 nm, which is consistent with the fiber diameters found in helicoids of other arthropod species. The longitudinal, transverse, and shear modulus of the nanofiber were determined to be 710 MPa, 70 MPa, and 90 MPa, respectively. The established experimental-theoretical methodology promises to be a useful tool for nanoscale characterization of helicoidal and other structures found in biological materials.

1. Introduction

Millions of years of evolution have produced fascinating biological materials and structures that are optimized to perform a wide spectrum of functions essential for the survival of organisms. These biological materials have been intensively studied in order to decipher the intricate interplay between their superior material properties and structural design principles. For instance, studies performed on abalone nacre revealed that the material exhibits a toughness similar to aluminum even when it contains 95% calcite, a ceramic.[1] Espinosa and co-workers showed that such toughness arises from a millimeter size process zone consisting of tablets sliding without pullout.[2,3] Recent developments in advanced manufacturing such as freeze casting and 3D printing have made possible the direct translation of the elegant architectures from natural materials to artificial materials and structures. More importantly, the new technologies have pushed the sizes of building elements to an even smaller scale for biomimicry.[4] These advances put further requirements on the characterizations of the structural and material properties of natural materials, which has always been challenging since most natural materials are anisotropic and composed of complex hierarchies across several length scales.

The exoskeletons of crustaceans and beetles are of significant interest due to their multifunctional properties, such as supporting the animal's body weight and resisting predator attacks and environmental damage while enabling locomotion.[5–7] The core region inside the exoskeletons is composed of chitin fibrils arranged in a helicoidal stacking, which is also known as Bouligand type or twisted plywood structures.[8] Characterization of the Bouligand structure along with the constituent fiber properties is essential for understanding the intriguing structure-function relationship. For example, using diffraction contrast transmission electron microscopy, Giraudguille et al. characterized the Bouligand structure in the cuticle of a crab and discussed the morphology of the crystalline chitin and its surrounded protein.[9] In other studies, Raabe and co-workers presented the plywood arrangements of chitin-protein fibers in lobster samples by analyzing X-ray diffraction patterns.[10,11] Compared to crustacean cuticles in which the fibrous structures are mineralized, beetle cuticle is almost purely polymeric and the Bouligand structure inside generally appears at a smaller length scale.

Beetle cuticle has been extensively investigated to gain insight into its various functions.[6] Such studies showed that the mechanical properties of its constituents play key roles in the remarkable mechanical performance of the system. An example is the efficient wing attachment, consisting of elastic hinges and wear resistant articulations,[12] that affect aerodynamic performance[13] and fatigue life.[14] Hence, characterization of cuticle structure, as an inspiring structural composite

R. Yang,[+] A. Zaheri, W. Gao,[++] Prof. H. D. Espinosa
Department of Mechanical Engineering
Northwestern University
Evanston, IL 60062, USA
E-mail: espinosa@northwestern.edu
A. Zaheri, W. Gao, Prof. H. D. Espinosa
Theoretical and Applied Mechanics Program
Northwestern University
Evanston, IL 60062, USA
Prof. C. Hayashi
Department of Biology
University of California
Riverside, CA 92521, USA
[+]Present address: Department of Mechanical and Materials Engineering, University of Nebraska-Lincoln, Lincoln, NE 68588, USA
[++]Present address: Department of Mechanical Engineering, University of Texas at San Antonio, San Antonio, TX 78249, USA

DOI: 10.1002/adfm.201603993

system, requires identification of geometrical and mechanical properties across spatial scales. For the exocuticle's Bouligand structure, this corresponds to pitch and angle of rotation between fibers in each layer[15] as well as stiffness and strength of the fibers. Previous studies made use of polarized microscopy,[16] scanning electron microscopy,[17] and transmission electron microscopy[15] to examine the helicoidal arrangement of fibers. However, to the best of our knowledge, the anisotropic elastic properties of the fibers in the Bouligand structure have not been identified.

Besides mechanical properties, other interesting features in beetles that also originate from the Bouligand structure are the iridescence of the cuticle and its structural coloration.[18,19] Specifically, many beetles have elytra (hardened forewings) with brilliant colors and metallic appearances. Such optical response of elytra has been studied by investigators in recent years.[20–24] Recognition of different forms of photonic crystal structures in natural biomaterials will likely inspire scientists to manufacture nonlinear optical devices. The basis for these optical properties of elytra is the periodic helicoidal structures where the layers show selective reflection for circularly polarized light. To examine this behavior, one needs knowledge about the nanoscale architecture such as the helicoidal pitch and angle of rotation between layers.[25]

In this paper, we present an atomic force microscopy (AFM)-based characterization method to identify the Bouligand structure inside beetle cuticle. We employ not only the high image resolution of the AFM, but also perform nanoindentation experiments to identify the anisotropic elastic properties of the constituent fiber by means of anisotropic contact mechanics analysis. The methodology is general and can be applied to the study of other types of biocomposites that have features with characteristic dimensions of less than 100 nm.

2. Results and Discussion

The beetle, *Cotinis mutabilis* (Cetoniinae), a field crop pest in the western U.S., was studied as a model system in this paper. As shown in **Figure 1**a, the exoskeleton of the adult male is 2 cm in length and 1 cm in width. The optical image of the cross section of the exoskeleton (Figure 1b), taken in the longitudinal direction, shows three structural layers: epicuticle, exocuticle, and endocuticle. At the bottom, there are periodic voids bridged by trabeculae, a typical lightweight design found in nature.[26] The epicuticle layer is the outermost part of the cuticle with a thickness of less than 10 µm, which mainly consists of wax, protein, and lipids, and acts primarily as an environmental barrier. The procuticle includes both the exocuticle and endocuticle, and is made of chitin fibers embedded in a proteinaceous matrix.[27,28] The endocuticle, formed during metamorphosis of larvae into adult beetles, provides rigidity and strength to the exoskeleton. The brick-like pattern on the sectioned surface of the endocuticle, as shown in Figure 1c, arises from cutting bundles of fibers along different orientations. By contrast, the exocuticle, developed in larval beetles,[29]

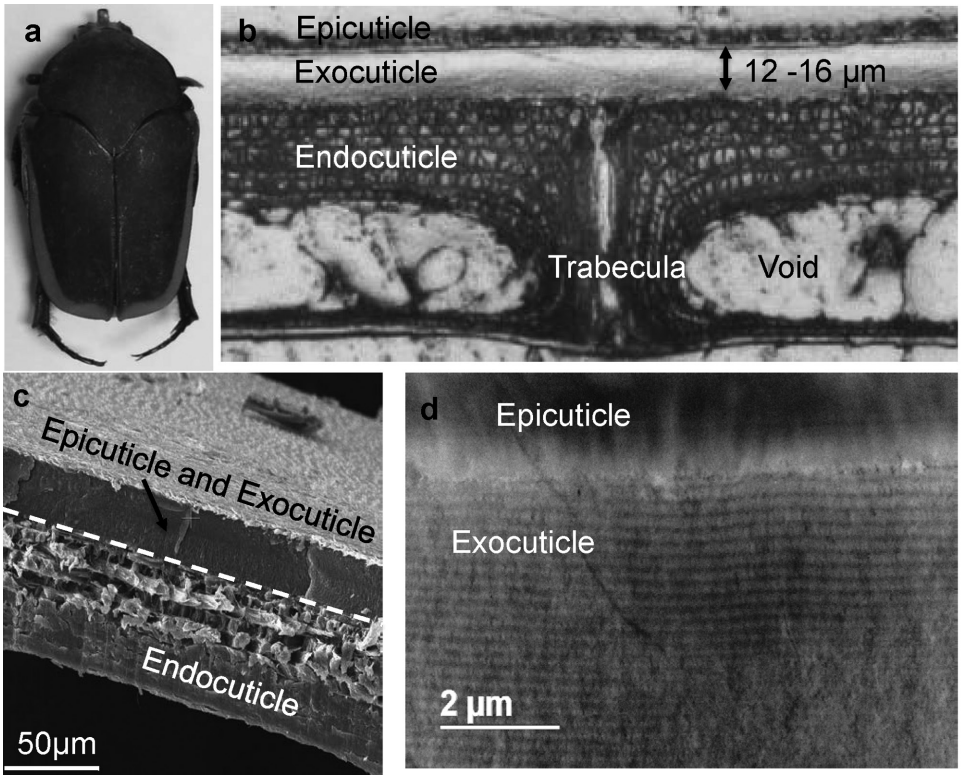

Figure 1. Images of the beetle exoskeleton. a) Male adult of *Cotinis mutabilis*. b) Optical image of the cross-section of the beetle exoskeleton with the epicuticle, exocuticle, and endocuticle visually defined by grayscale contrast. c) SEM image of the flat fractured surface of the epicuticle and exocuticle, and the brick-like structure of the endocuticle. d) STEM image of the multilayered pattern of the exocuticle, with estimated layer thickness of ≈220 nm.

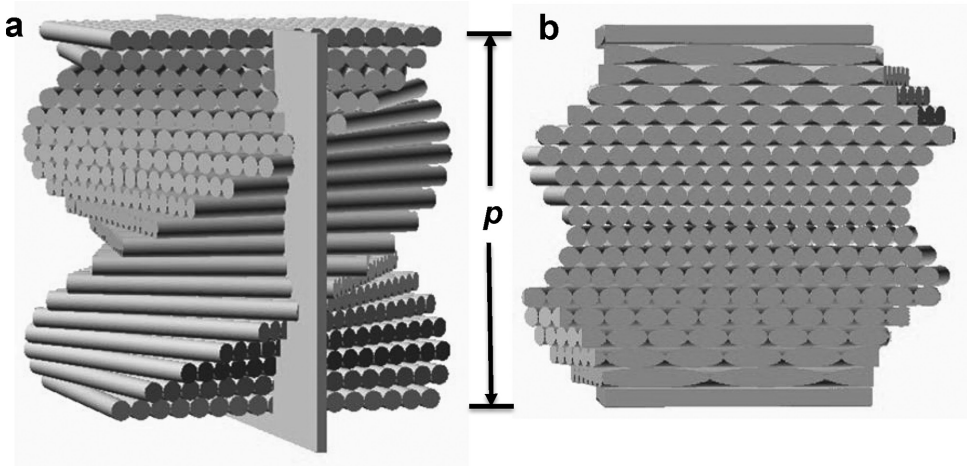

Figure 2. Schematic drawing of the helicoidal structure. a) Depiction of helicoidal structure with 18 layers within one pitch (size p). b) The 90° cross-section cut by the plane shown in (a), on which AFM scanning and indention was performed.

does not show any observable features at this scale, suggesting a finer structure. Interestingly, the scanning transmission electron microscopy (STEM) image of the exocuticle cross-section, shown in Figure 1d, reveals a layered periodic structure with a periodicity estimated to be 220 nm.

This exocuticle layered pattern (STEM image, Figure 1d) is consistent with the helicoidal Bouligand structure that was suggested by previous studies.[9] **Figure 2** shows a schematic of the helicoidal structure, which is composed of many layers of fibers, stacked with a constant twist angle θ, with each layer consisting of fibers aligned in the same orientation.[30] The total number of layers n in one pitch (a distance for a rotation of π) can be calculated as

$$n = p/d \tag{1}$$

where p is the pitch length and d is the diameter of a single fiber. Then, the twist angle between two adjacent layers can be written as

$$\theta = \pi/n \tag{2}$$

Considered to be the fundamental building blocks of the helicoidal structure, the fibers are bundles of chitin polymer chains wrapped with proteins.[31] Owing to this chain structure, each fiber has a larger modulus along the axial or longitudinal direction than that along the transverse direction. Thus, an individual fiber can be approximately considered as a transversely isotropic material with five independent elastic constants, as suggested by previous studies.[32] It is quite challenging to characterize these elastic constants when the fibers, possessing nanoscale dimensions, are embedded within a matrix. In the following sections, we discuss an approach that combines AFM-based nanoindentation and anisotropic indentation analysis to identify the dimension of individual fibers as well as their elastic properties.

First, the topography of a surface sectioned 90° with respect to the longitudinal direction of the elytra is characterized by AFM with a scan size of 980 nm × 980 nm. As shown in **Figure 3**a, the scan exhibits periodic alternating dark and light contrasts, and notably the line section on the image (Figure 3b) shows that the periodicity of this pattern is around 200 nm, which is consistent with the length of the helicoidal pitch (≈220 nm) estimated from the STEM image (Figure 1d). It is also worth noting that there is significant nonuniformity of the layer thickness. Moreover, it can be clearly seen from Figure 3 that each pitch is closely packed with circularly shaped features generated from the cross-section of individual fibers. The height of each cluster depends on the fiber orientation, as schematically illustrated in Figure 2b. We analyzed the topographical images to identify the dimension of these circular-shaped features. As shown in Figure 3c, the image is partitioned into many small units with closed contours according to the topographical contrast. Then, based on the areas of these units, the equivalent circular diameters are calculated and plotted in Figure 3d. The averaged diameter of the fiber, d is estimated to be around 20–30 nm. This value is in good agreement with values reported for the chitin-protein fibers in other beetles.[15] From Equations (1) and (2), one can estimate a total of around n = 10–15 fiber layers stacked to make an individual pitch, leading to a rotation angle between adjacent fibers of around θ = 12°–18°. Furthermore, we note that the topological difference on the scanned surface can be attributed to the fiber's anisotropic mechanical property. Fibers that are sectioned perpendicular to their axial direction would have more protrusions upon the scanned surface due to the larger longitudinal modulus of the fibers. This can be further confirmed by our AFM-based nanoindentation on the sectioned surface.

The AFM-based nanoindentation was performed on a series of points along a single pitch, as shown in Figure 3c. A typical force–displacement curve is shown in **Figure 4**a, in which the maximum applied force was around 150 nN with a displacement of 200 nm. The displacement is the subtraction between the travel distance of the piezo actuator and the vertical deflection of the cantilever. The contact stiffness, S, is obtained as the slope at the inception of the unloading curve. Vlassak et al.[33] showed that S can be written as

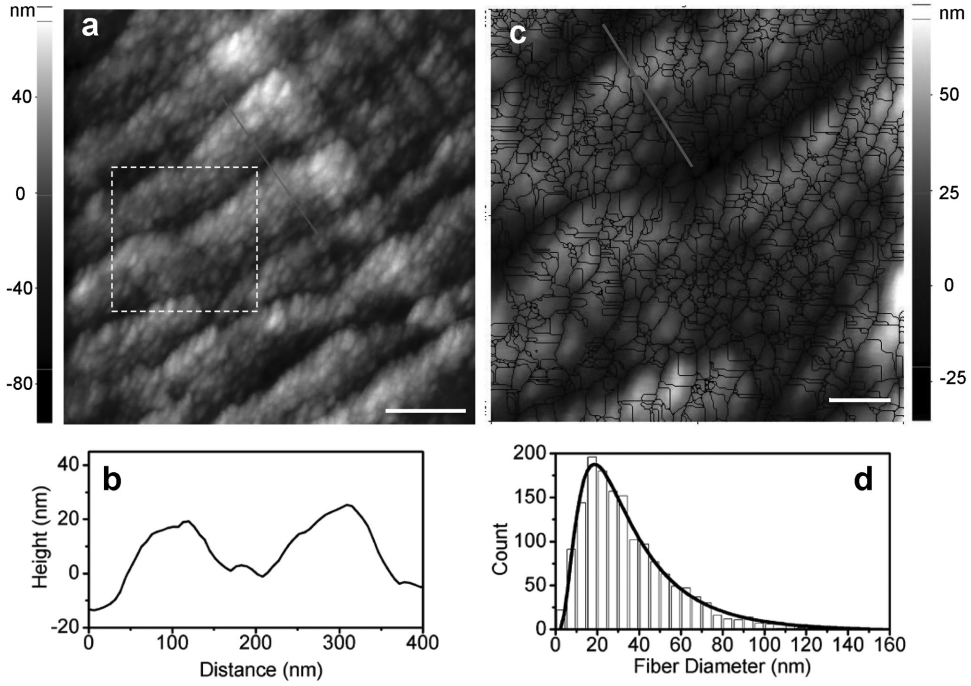

Figure 3. AFM images identifying the Bouligand structure in the exocuticle. a) Tapping mode image of exocuticle showing approximately seven nonuniform pitches (scale bar: 200 nm). b) Height profile of the line section in (a). c) Zoom-in image of the region within the white-dashed box in (a). According to the topographical contrast, the image is partitioned into small units with closed contours, which indicate the cross-sections of individual fibers (scale bar: 50 nm). Nanoindentation was performed following the line shown in c) to obtain the indentation modulus within one pitch (Figure 4b). d) Fiber diameter distributions identified from the image shown in (c).

$$S = \frac{dF}{dU} = \frac{2}{\sqrt{\pi}} M \sqrt{A_C} \tag{3}$$

where F is the applied load, U is the vertical displacement of the indenter, and A_C is the projected contact area. M, defined as the indentation modulus, is a function of elastic constants and, in general, dependent on the shape of the indenter. For isotropic materials and axisymmetric geometries, M can be simplified to reduced modulus $E/(1-\nu^2)$. To experimentally determine the indentation modulus from Equation (3), we have to estimate the projected area of contact, which is an elliptic shape in the case of anisotropic materials. The estimation of the contact ellipse area A_C based on the analysis from Swadener and Pharr is given by[34]

$$A_C = 2\pi R U_C \tag{4}$$

where R is the radius of the indenter, and U_C is the mean contact depth averaged over the perimeter of contact. The value of U_C can be calculated using Oliver–Pharr method as[35]

$$U_C = U_{max} - \varepsilon \frac{F_{max}}{S} \tag{5}$$

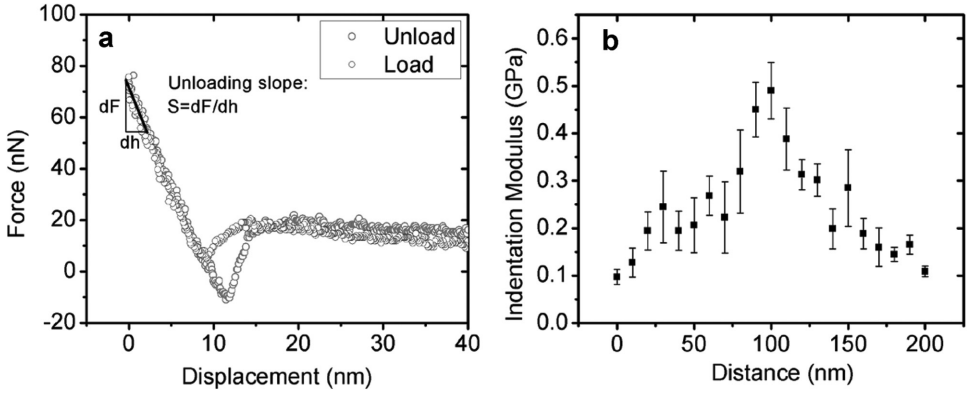

Figure 4. AFM-based nanoindentation in the exocuticle. a) Representative force–displacement curves from nanoindentation. b) Indentation moduli, obtained from the unloading curve, are plotted as a function of distance over one pitch following the line shown in Figure 3c.

where U_{max} and F_{max} are, respectively, the maximum indentation depth and force at the onset of unloading. The factor ε can be estimated as 0.75 for spherical indentation to the first order approximation.[36] It is noted that Equation (5) was initially proposed for isotropic materials but can be extended for anisotropic materials. Using Equations (3)–(5), we can calculate the values of indentation modulus. The values of indentation moduli as a function of line scan distance along one pitch are shown in Figure 4b. Since there are roughly six fiber layers within a 90° half pitch, the neighboring data points in Figure 4b were averaged to have six points (in **Figure 5**b) for the anisotropic contact mechanics analysis. Note that the modulus exhibits the same periodicity as what is measured from the topological scan. Moreover, the modulus has the highest value when the indentation direction is aligned with the fiber axial direction, and it gradually decreases when the indentation direction moves toward the fiber radial direction, which agrees with the transverse anisotropy of the fiber.

Next, we identified the anisotropic material properties based on the measured indentation modulus. As shown in Figure 5a, the fiber is considered as a transversely isotropic material with stiffness tensor C_{ijkl} defined in a Cartesian coordinate system ($\mathbf{e}_1$, $\mathbf{e}_2$, $\mathbf{e}_3$), where $\mathbf{e}_i$ denotes the unit vector on the ith direction. $\mathbf{e}_1$ is aligned with the axial direction of the fiber, and $\mathbf{e}_3$ lies in the sectioned plane along the Bouligand stacking direction. It is noted that the direction of the major axis of the contact ellipse coincides with the $\mathbf{e}_3$ direction due to the nature of the transverse material property. The indentation direction n is normal to the cross-section, and the angle γ between n and $\mathbf{e}_1$ describes the orientation of the fiber. To establish the relationship between elastic constants of the material and indentation modulus, we employed the method proposed by Vlassak et al.[33] Such a method has been successfully applied to study the conical indentation on wood cell walls.[37] The method is based on the surface Green's function for anisotropic materials proposed by Barnett and Lothe.[38] Upon a unit load on the indentation direction n, the displacement of a point P at a position r on the surface is given by

$$w(\mathbf{r}) = \frac{1}{8\pi^2 r}\left[n_j B_{jk}^{-1}(\mathbf{e}_3^*) n_k\right] = \frac{h(\theta)}{r} \tag{6}$$

where n_j are the components of unit vector $\mathbf{n}$, and $\mathbf{e}_3^*$ is the unit vector along vector $\mathbf{r}$. $w(\mathbf{r})$ is inversely proportional to the distance r, and has an angle-dependent part $h(\theta)$, where θ is defined as the angle between $\mathbf{e}_3$ and $\mathbf{e}_3^*$. The function $h(\theta)$ is related to a symmetric and positive definite second order tensor B, which is defined by

$$B_{jk}^{-1}(\mathbf{e}_3^*) = \frac{1}{8\pi^2}\int_0^{2\pi}\left[D_{jk}^{11} - D_{js}^{12} D_{sr}^{22} D_{rk}^{21}\right] \mathrm{d}\varphi \tag{7}$$

where

$$D_{jk}^{mn} = (e_m^*)_i C_{ijkl} (e_n^*)_l \tag{8}$$

Here, in order to compute tensor B, another Cartesian coordinate system $(\mathbf{e}_1^*, \mathbf{e}_2^*, \mathbf{e}_3^*)$ is constructed by three sequential rotations from the original coordinate ($\mathbf{e}_1$, $\mathbf{e}_2$, $\mathbf{e}_3$): the first rotation from $\mathbf{e}_1$ to $\mathbf{n}$ about $\mathbf{e}_3$ by angle γ, the second rotation from $\mathbf{e}_3$ to $\mathbf{e}_3^*$ about $\mathbf{n}$ by angle θ, and the final rotation from $\mathbf{n}$ to $\mathbf{e}_1^*$ about $\mathbf{e}_3^*$ by angle φ. Note that the components of unit vectors $\mathbf{e}_m^*$ and elastic tensor C in Equation (8) are expressed in coordinate ($\mathbf{e}_1$, $\mathbf{e}_2$, $\mathbf{e}_3$). Based on the surface green function, the relation between indentation force F and indentation displacement U is given by

$$F(e) = \frac{4U^{3/2}}{3\alpha(e)\sqrt{C\left(2-e^2\right)}} \tag{9}$$

where the constant C is related to the geometry of the indenter, and $\alpha(e)$ is a function of the eccentricity of the contact ellipse $\left(e = \sqrt{1-b^2/a^2}\right)$, which is given by

$$\alpha(e) = \int_0^{\pi} \frac{h(\theta)}{\sqrt{1-e^2\cos^2\theta}} \mathrm{d}\theta \tag{10}$$

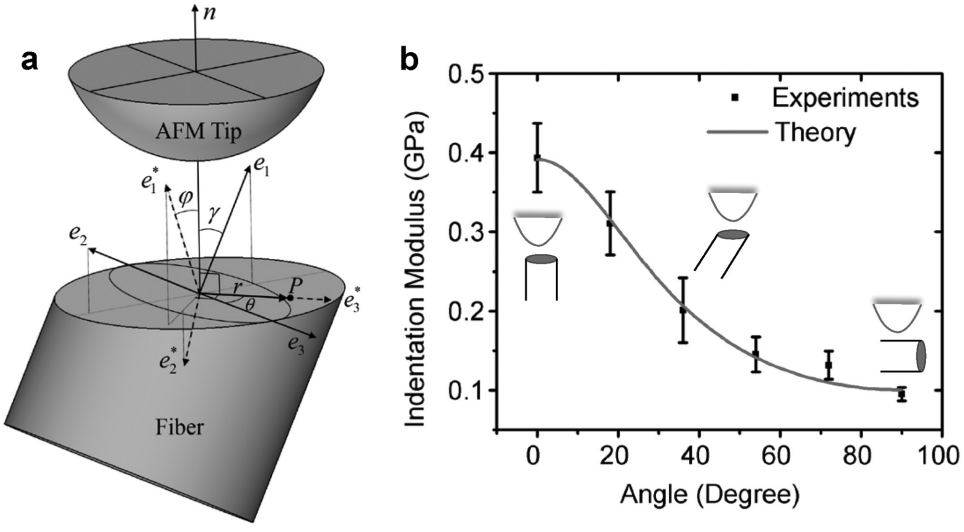

Figure 5. Contact mechanics analysis of beetle fiber's anisotropic elastic properties. a) Coordinate systems used for contact mechanics analysis. b) Indentation moduli from experiment are compared to the values predicted from contact mechanics analysis.

where $h(\theta)$ is obtained from Equation (6). According to Barber's theorem,[39] for a given indention depth, the eccentricity e is that which maximizes the indentation force F under the Rayleigh–Ritz approximation. This is equivalent to finding the value of e that minimizes the term $\alpha(e)\sqrt{(2-e^2)}$ in Equation (9). Then, the contact stiffness can be derived as

$$S = \frac{\mathrm{d}F}{\mathrm{d}U} = \frac{2}{\sqrt{\pi}}\sqrt{A_C}\,\frac{1}{\alpha(e)(1-e^2)^{1/4}} \tag{11}$$

By comparing Equation (11) and Equation (3), the indentation modulus can be written as

$$M^{\mathrm{T}} = \frac{1}{\alpha(e)(1-e^2)^{1/4}} \tag{12}$$

where the M^{T} is used to differentiate from the indentation modulus M measured from experiment.

Equation (12) provides the relationship between indentation modulus and elastic constants of the material. The fiber is transversely isotropic with five independent elastic constants, namely, E_{l}, E_{t}, G_{tl}, ν_{tt}, and ν_{tl}, where subscripts l and t refer to the longitudinal and transverse direction of the fiber. The identification of the elastic constants of the fiber is based on an error minimization procedure, which has been applied previously to study the mechanical properties of wood cell walls.[37] As noted in conventional indentation problems, the influence of two Poisson's ratio on the indentation modulus are negligible compared to the influence of the other three elastic moduli. Therefore, only three elastic moduli are considered in the error minimization calculation, while both Poisson's ratios are set to 0.3. As such, the error η can be defined by

$$\eta = \sqrt{\sum_{i=1}^{n}\left(M(\gamma_i) - M_i^T\left(E_1, E_2, G, \gamma_i\right)\right)^2} \tag{13}$$

where γ_i describe different orientations of fiber with respect to the indentation direction (see Figure 5a). As previously mentioned, for the material under investigation, there are about six fibers across half of the Bouligand structure period, thus there are six points when the indentation angle varies from 0° to 90°. Minimization of Equation (13) leads to longitudinal, transverse, and shear moduli of 710, 70, and 90 MPa, respectively. With these elastic constants, the indentation moduli M^{T} are computed and compared with experimental measurements in Figure 5b. The identified moduli of fibers are within the range of the values reported previously for the insect cuticle (0.1 and 1 GPa),[40] but it is noted that the present method allows for identification of material anisotropy by taking advantage of the helicoidal feature inside the cuticle.

The anisotropy of the fiber, as indicated by the ratio between the maxima and minima of the moduli, comes from the atomistic structure of chitin chains inside the fiber. The covalent bonded backbone along the chain direction results in a much higher elastic modulus, as compared to the one perpendicular to the chain direction.[32] The anisotropy from chitin chains is reduced when the chains are wrapped by soft protein complexes to form fibers. Moreover, as discussed in a previous study on lobster cuticle,[32,41] the level of mineralization in cuticle strongly affects the anisotropic material property, since the absorption of inorganic particles to the polymeric structure increases the material isotropy. As a result, the fibers in beetle cuticle, mostly composed by polymeric materials, exhibit higher level of anisotropy than the cuticles in crustaceans such as mantis shrimp, crab, and lobster, which also possess a helicoidal structure but contains abundant inorganic materials.[32,41,42] The heavy presence of inorganic materials in crustaceans also results in much larger elastic moduli[43,44] as compared with the values obtained on beetles. Since the mineralization level in beetle exocuticle is very low,[45] consistent with our AFM data in Figure 3 that show a tight packing of soft fibers in each layer of exocuticle, we consider that homogenization is not required in our analysis. It is noted that, in comparison to previous indentation experiments on lobster cuticle conducted with a classical nanoindenter,[46] we used AFM with a sharp tip to perform the indentation, since the beetle cuticle requires much finer indentation resolution due to the nature of its structure. Moreover, we were not only able to observe the material anisotropy, but also obtained the material properties by combining experimental measurements with anisotropic indentation theory.

The Bouligand fibrous arrangements in general can improve mechanical properties and provide the structure with adaptability to the loading environment.[47] For example, one of the effects of this architectural arrangement is to enhance the material toughness by deflecting the paths of crack propagation.[48] Another effect is the shear wave filtering capability exhibited when the material is subjected to dynamic loads.[43] Understanding these mechanisms requires fine characterization of the Bouligand structure and materials, such as the present method developed on the beetle exocuticle.

The methods and findings we have derived from studying *C. mutabilis* exoskeleton can be extended to other beetle species. For example, correlating mechanical properties with the geometries of exocuticle and endocuticle layers from diverse beetle species will use the results of natural selection to better understand structure/function of exoskeleton architecture. Coleoptera (beetles) is the largest order of insects and the millions of beetle species vary greatly from each other in taxonomic relatedness, body size, and ecology (e.g., diet, locomotor ability, predation pressure). Comparison of beetles with different demands on their exoskeleton is expected to reveal insights into how natural selection has shaped nanofiber composition, spatial scale, and orientation.

The current study focuses on the exocuticle layer with Bouligand structure, but to understand the properties of the whole exoskeleton requires studies on other layers as well, such as the endocuticle. It can be seen from Figure 1c that the exocuticle and endocuticle layers have different structural architectures, although they appear to share the same building blocks, i.e., chitin fibers. Here, we also performed high resolution AFM imaging on the endocuticle, as shown in **Figure 6**. Interestingly, we found that the nanofibers of endocuticle and exocuticle have similar diameters, but the nanofibers in endocuticle are arranged orthogonally with only two orientations rather than helicoidally with many layers as in the exocuticle. Further, the image seems to show a transition layer from exocuticle to endocuticle. It is important to understand why and how the beetle exoskeleton evolved such elegant structures, and additionally,

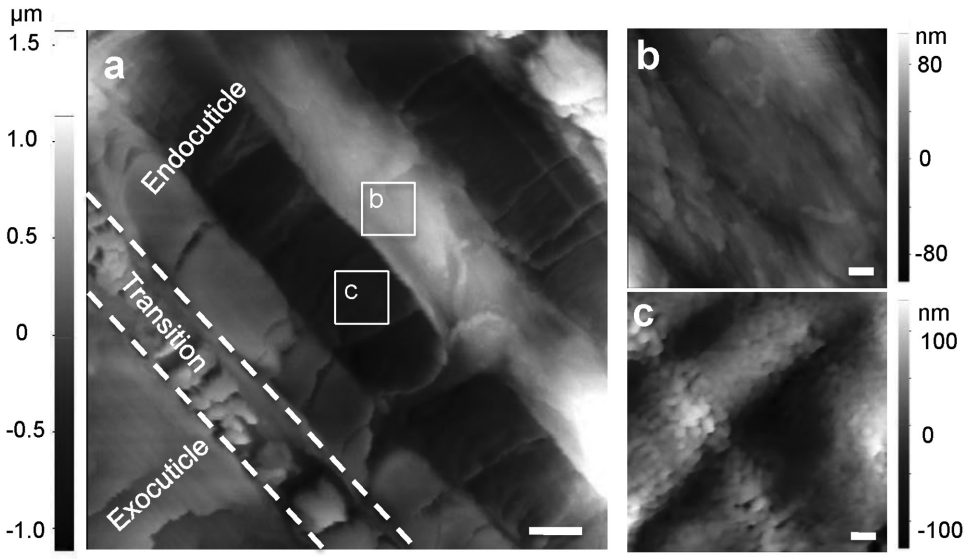

Figure 6. AFM images of beetle endocuticle. a) The band-shaped configuration reveals the orthogonal fiber arrangement in the endocuticle (scale bar: 2 μm). The light bands, almost parallel to the aligned fibers, are zoomed-in (b) (scale bar: 200 nm). The dark bands, almost perpendicular to the fibers (with diameters of 20–40 nm), are zoomed-in (c) (scale bar: 100 nm).

how to learn the underlying principles for advanced material design. The AFM nanoindentation based method developed here will be useful for such studies. The detailed investigations on the endocuticle and the transition layer as well as the integrated structural performance are left for future studies.

3. Conclusions

Quantification of pitch size, diameter, and twisting angle, as well as the anisotropic elastic constants of the constituent fibers of *C. mutabilis* cuticle was performed using an experimental–theoretical framework that combines AFM nanoindentation and anisotropic contact mechanics analysis. This approach provided direct characterization of beetle cuticle at the nanoscale and enabled identification of the fiber-matrix structural arrangement. Determination of the material properties of the constitutive elements will provide insight into how a particular fibrous arrangement evolved to achieve a particular mechanical behavior. Thus, further studies across beetle species should be carried out to understand the formation of fiber structures as well as the diversity of cuticle designs and properties. The methodology developed here can in principle be applied not only to beetles but also broadly to other animal and plant taxa to reveal their fibrous arrangements as well as material properties. Such work will bring us closer to answering questions about *how* particular fiber arrangements relate to mechanical properties as well as questions about *why* particular fiber arrangements evolved.

4. Experimental Section

Sample Preparation: Male, adult specimens of *C. mutabilis* beetle were acquired from BioQuipBugs.com. Upon arrival, all specimens were received air-dried. To investigate the elytra structure and its mechanical properties, in particular the cuticle layers, small rectangular samples were cut from the insect specimens with double-edge razor blades. Samples for light optical microscopy were embedded in epoxy (EpoThin 2) and then polished with different grits from 35 μm down to sub-micrometer. Samples for scanning electron microscopy (SEM) were mounted onto aluminum stubs with double-sided adhesive conductive carbon tape, sputter coated with 8 nm osmium, and viewed in a Nova NanoSEM 600 (FEI Co., Hillsboro, OR, USA). Samples for STEM were fixed with 2.5% glutaraldehyde, stained, and fixed with 2% osmium tetroxide dehydrated in ethanol and infiltrated in ethanol-resin mixture as well as pure resin. Finally, the treated samples were polymerized in fresh resin for 48 h at 65 °C. Samples for AFM were similarly prepared. Cured blocks containing the samples were trimmed and sectioned normally to the outer surface in 200 nm thick slices using an ultramicrotome (Leica UC7/FC7 Cryo-Ultramicrotome). The sections for AFM were placed on a glass slide, and the ones for STEM were collected onto formvar carbon-coated copper grids and observed with a Hitachi HD-2300 STEM.

Atomic Force Microscopy: Sectioned beetle cuticle samples were imaged with the Park Systems XE-120 AFM (Park Systems, Santa Clara, CA) using noncontact mode. A silicon probe from Bruker Nano Surface (Santa Barbara, CA) was used with a nominal spring constant of 42 N m^{-1} and nominal tip apex diameter of 20 nm. The precise spring constant was calibrated with thermal tune method before each experiment. Nanoindentation experiments were performed with the same probe under contact mode.

Acknowledgements

R.Y., A.Z., and W.G. contributed equally to this work. The authors gratefully acknowledge financial support from a Multi-University Research Initiative through the Air Force Office of Scientific Research (AFOSR-FA9550-15-1-0009). This work made use of the EPIC, Keck-II, and SPID facilities of the NUANCE Center at Northwestern University. The authors also thank Dr. Reiner Bleher and Dr. Benjamin Russell for helpful discussions.

Received: August 5, 2016
Revised: October 28, 2016
Published online:

[1] H. J. Gao, B. H. Ji, I. L. Jager, E. Arzt, P. Fratzl, *Proc. Natl. Acad. Sci. USA* **2003**, *100*, 5597.
[2] D. Gregoire, O. Loh, A. Juster, H. D. Espinosa, *Exp. Mech.* **2011**, *51*, 591.
[3] H. D. Espinosa, A. L. Juster, F. J. Latourte, O. Y. Loh, D. Gregoire, P. D. Zavattieri, *Nat. Commun.* **2011**, *2*, 173.
[4] U. G. K. Wegst, H. Bai, E. Saiz, A. P. Tomsia, R. O. Ritchie, *Nat. Mater.* **2015**, *14*, 23.
[5] J. C. Weaver, G. W. Milliron, A. Miserez, K. Evans-Lutterodt, S. Herrera, I. Gallana, W. J. Mershon, B. Swanson, P. Zavattieri, E. DiMasi, D. Kisailus, *Science* **2012**, *336*, 1275.
[6] J. F. V. Vincent, U. G. K. Wegst, *Arthropod Struct. Dev.* **2004**, *33*, 187.
[7] K. Okumura, *MRS Bull.* **2015**, *40*, 333.
[8] Y. Bouligand, *Tissue Cell* **1972**, *4*, 189.
[9] M. M. Giraudguille, H. Chanzy, R. Vuong, *J. Struct. Biol.* **1990**, *103*, 232.
[10] A. Al-Sawalmih, C. H. Li, S. Siegel, H. Fabritius, S. B. Yi, D. Raabe, P. Fratzl, O. Paris, *Adv. Funct. Mater.* **2008**, *18*, 3307.
[11] F. Bobelmann, P. Romano, H. Fabritius, D. Raabe, M. Epple, *Thermochim. Acta* **2007**, *463*, 65.
[12] S. N. Gorb, *Int. J. Insect. Morphol.* **1998**, *27*, 205.
[13] P. E. Sitorus, H. C. Park, D. Byun, N. S. Goo, C. H. Han, *J. Bionic Eng.* **2010**, *7*, 354.
[14] H. Hepburn, A. Ball, *J. Mater. Sci.* **1973**, *8*, 618.
[15] L. Cheng, L. Y. Wang, A. M. Karlsson, *J. Mater. Res.* **2009**, *24*, 3253.
[16] S. A. Jewell, P. Vukusic, N. W. Roberts, *New J. Phys.* **2007**, *9*, 99.
[17] B. Chen, X. Peng, C. Cai, H. Niu, X. Wu, *Mater. Sci. Eng., A* **2006**, *423*, 237.
[18] T. Lenau, M. Barfoed, *Adv. Eng. Mater.* **2008**, *10*, 299.
[19] X. Wu, A. Erbe, D. Raabe, H. O. Fabritius, *Adv. Funct. Mater.* **2013**, *23*, 3615.
[20] J. Hwang, M. H. Song, B. Park, S. Nishimura, T. Toyooka, J. W. Wu, Y. Takanishi, K. Ishikawa, H. Takezoe, *Nat. Mater.* **2005**, *4*, 383.
[21] J. W. Galusha, L. R. Richey, J. S. Gardner, J. N. Cha, M. H. Bartl, *Phys. Rev. E* **2008**, *77*, 050904.
[22] A. E. Seago, P. Brady, J. P. Vigneron, T. D. Schultz, *J. R. Soc., Interface* **2009**, *6*, S165.
[23] V. Sharma, M. Crne, J. O. Park, M. Srinivasarao, *Science* **2009**, *325*, 449.
[24] M. Burresi, L. Cortese, L. Pattelli, M. Kolle, P. Vukusic, D. S. Wiersma, U. Steiner, S. Vignolini, *Sci. Rep.* **2014**, *4*, 1.
[25] B. D. Wilts, H. M. Whitney, B. J. Glover, U. Steiner, S. Vignolini, *Mater. Today: Proc.* **2014**, *1*, 177.
[26] J. x. Chen, Q. q. Ni, Y. Endo, M. Iwamoto, *Entomologia Sinica* **2002**, *9*, 55.
[27] Y. Arakane, J. Lomakin, S. H. Gehrke, Y. Hiromasa, J. M. Tomich, S. Muthukrishnan, R. W. Beeman, K. J. Kramer, M. R. Kanost, *PLoS Genet.* **2012**, *8*, 612.
[28] S. F. Liu, J. Sun, L. N. Yu, C. S. Zhang, J. Bi, F. Zhu, M. J. Qu, C. Jiang, Q. L. Yang, *Molecules* **2012**, *17*, 4604.
[29] D. Gennard, *Forensic Entomology: An Introduction*, John Wiley & Sons, Chichester, UK **2012**.
[30] D. Raabe, C. Sachs, P. Romano, *Acta Mater.* **2005**, *53*, 4281.
[31] D. Raabe, P. Romano, C. Sachs, H. Fabritius, A. Al-Sawalmih, S. Yi, G. Servos, H. G. Hartwig, *Mater. Sci. Eng. A* **2006**, *421*, 143.
[32] S. Nikolov, M. Petrov, L. Lymperakis, M. Friak, C. Sachs, H. O. Fabritius, D. Raabe, J. Neugebauer, *Adv. Mater.* **2010**, *22*, 519.
[33] J. J. Vlassak, M. Ciavarella, J. R. Barber, X. Wang, *J. Mech. Phys. Solids* **2003**, *51*, 1701.
[34] J. G. Swadener, G. M. Pharr, *Philos. Mag. A* **2001**, *81*, 447.
[35] W. C. Oliver, G. M. Pharr, *J. Mater. Res.* **2004**, *19*, 3.
[36] M. P. Wenger, L. Bozec, M. A. Horton, P. Mesquida, *Biophys. J.* **2007**, *93*, 1255.
[37] A. Jager, T. Bader, K. Hofstetter, J. Eberhardsteiner, *Composites, Part A* **2011**, *42*, 677.
[38] D. M. Barnett, J. Lothe, *Phys. Norv.* **1975**, *8*, 13.
[39] J. Barber, *J. Strain Anal. Eng. Design* **1974**, *9*, 230.
[40] U. G. K. Wegst, M. F. Ashby, *Philos. Mag.* **2004**, *84*, 2167.
[41] S. Nikolov, H. Fabritius, M. Petrov, M. Friak, L. Lymperakis, C. Sachs, D. Raabe, J. Neugebauer, *J. Mech. Behav. Biomed.* **2011**, *4*, 129.
[42] H. O. Fabritius, A. Ziegler, M. Friak, S. Nikolov, J. Huber, B. H. M. Seidl, S. Ruangchai, F. I. Alagboso, S. Karsten, J. Lu, A. M. Janus, M. Petrov, L. F. Zhu, P. Hemzalova, S. Hild, D. Raabe, J. Neugebauer, *Bioinspir. Biomim.* **2016**, *11*, 055006.
[43] N. Guarin-Zapata, J. Gomez, N. Yaraghi, D. Kisailus, P. D. Zavattieri, *Acta Biomater.* **2015**, *23*, 11.
[44] H. O. Fabritius, E. S. Karsten, K. Balasundaram, S. Hild, K. Huemer, D. Raabe, *Z. Kristallogr.* **2012**, *227*, 766.
[45] M. C. Verkerk, J. Tramper, J. C. M. van Trijp, D. E. Martens, *Biotechnol. Adv.* **2007**, *25*, 198.
[46] C. Sachs, H. Fabritius, D. Raabe, *J. Mater. Res.* **2006**, *21*, 1987.
[47] E. A. Zimmermann, B. Gludovatz, E. Schaible, N. K. N. Dave, W. Yang, M. A. Meyers, R. O. Ritchie, *Nat. Commun.* **2013**, *4*, 1.
[48] M. A. Meyers, J. McKittrick, P. Y. Chen, *Science* **2013**, *339*, 773.